THE ASTROPHYSICAL JOURNAL, 291:52–62, 1985 April 1

SYNCHROTRON AGING IN THE LOBES OF LUMINOUS RADIO GALAXIES

STEVEN T. MYERS AND STEVEN R. SPANGLER
Department of Physics and Astronomy, University of Iowa
Received 1984 August 2; accepted 1984 October 16

ABSTRACT

We have made a study of the gradient of the 1.4–5.0 GHz spectral index observed in five luminous 3C radio galaxies. The observations have been compared with a model in which the radiation is due to an isotropic ensemble of electrons subject to synchrotron radiation losses (synchrotron aging). From such an analysis, we may infer the age (time since acceleration) of electrons at various locations in the lobes, and consequently speeds of separation of the hot spots and lobe material. The inferred speeds are typically in the range of (10–30) $\times 10^3$ km s^{-1}. The results are consistent with the beam model, in which the lobe material is left behind by a hot spot advancing through the intergalactic medium at speeds $\sim 10^4$ km s^{-1}. We discuss possible corrections to our speed estimates, and conclude that significantly higher speeds are possible, if not directly indicated. Finally, we present a number of graphs which should be useful to observers in the analysis of VLA spectral index data.

Subject headings: radio sources: galaxies — radio sources: spectra

I. INTRODUCTION

The structure of a luminous radio galaxy may be broadly categorized as consisting of a central component, a radio jet, hot spots, and extended lobes. Each of these features may be understood within the context of the widely accepted beam model (Blandford and Rees 1974) for the structure of double radio sources. The jets are believed to be fluid beams emanating from the central component. Hot spots are identified as a region of interaction between the beam and an intergalactic medium, and represent regions of electron acceleration. Finally, the extended lobes are populated by energetic electrons which "leak out" from the hot spot.

In this paper we will be concerned with the processes by which energetic electrons are transported from the hot spots into the lobes. In addition to being of interest in its own right, such a study can provide information regarding the beam model generally. A number of proposals have been made for processes by which this leakage occurs. In the simplest version of the beam model, the accelerated electrons are left behind by the advancing hot spot (Burch 1977, 1979; Winter *et al.* 1980). The speed of separation of the hot spot and a parcel of lobe material is then simply the speed at which the hot spot advances through the intergalactic medium.

More sophisticated versions of the beam model have resulted from recent numerical simulations (Norman *et al.* 1982; Norman, Winkler, and Smarr 1983). While in essential agreement with the aforementioned simple picture, these models furnish electron transport through a strong backflow, which acts in addition to the forward motion of the hot spot. As a result, the speed of separation of the hot spot and a parcel of lobe material is comparable to, but somewhat larger than, the hot spot of advance. Further discussion of these numerical models is given in § VII below.

There exist firm limits on the hot spot speed of advance. A fairly incontrovertible upper limit results from the work of Longair and Riley (1979). Using a sample of luminous double radio sources, they studied the distribution of distances from the central components to the hot spots. A limit of $0.2c$ was obtained for the average hot spot speed of advance. Recognition of the fact that environmental effects may also produce a difference in the distances of two hot spots from a central component leads us to conclude that Longair and Riley's result is probably a generous upper limit.

The hot spot speed of advance is also bounded from below. For the hot spot to be identified as a shock, it is obviously necessary for it to be moving faster than the speed of sound, which is $\sim 10^3$ km s^{-1} for a typical 10^8 K intergalactic medium. However, even higher hot spot speeds may be necessary. As noted by Longair and Riley (1979), the beam model requires that the hot spots be ram-pressure–confined by their motion through the intergalactic medium. High-resolution interferometric observations indicate that minimum energy densities in hot spots are of order 10^{-8} ergs cm^{-3} or greater (Lonsdale and Morison 1983). Even with the highest densities observed for intergalactic media, ram-pressure confinement requires hot spot speeds in excess of $0.05c$. It should be noted that this argument is based on one-dimensional calculations of pressure balance. Norman *et al.* (1982) comment that for more realistic two-dimensional calculations, such restrictions may not be applicable. For example, Norman *et al.* (1982) show (in Fig. 6 of their paper) that pressure in the hot spot can significantly exceed that expected from the dynamic pressure of the background medium. More investigation of this question is needed, but for this paper we will assume that hot spot speeds somewhat less than $0.05c$ are viable. We will adopt a range of (5–60) $\times 10^3$ km s^{-1} for the hot spot speed of advance. In the aforementioned simple model of energetic electron transport, this is equal to the speed of separation of the hot spot and an element of lobe material.

Quite different electron transport models, emphasizing energetic particle streaming, have been proposed by Spangler (1979), Spangler and Basart (1981), and Hughes (1979). In such models, electrons can stream out of the hot spot at speeds comparable to that of light. Such models do not take issue with the basis of the beam model, but contend that electrons, once accelerated, are free to move at high speeds. While we will not discuss the details of such models, a general characteristic is that the speed of separation of the hot spot and a radiating

electron is considerably greater than the hot spot speed of advance.

A plasma parameter of relevance to this discussion is the Alfvén speed. Plasma quasilinear theory predicts that particle streaming is limited to this speed (Wentzel 1974), so it might furnish a simple estimate of the backflow speed. Unfortunately, the Alfvén speed is a difficult quantity to determine observationally. Depolarization is frequently observed in radio sources, but it is unclear whether Faraday rotation is occurring in the emitting material (in which case the Alfvén speed can be determined) or in an external sheath. There is also uncertainty as to whether the magnetic field possesses a large-scale, static component or is completely random. Analyses predicated on the assumption that the depolarization is internal, and due to an ordered magnetic field, yield estimated Alfvén speeds of about 10^4 km s^{-1} (Spangler and Pogge 1984; Spangler, Myers, and Pogge 1984). As will be seen below, this value is comparable to other speed estimates.

Dual or multifrequency observations can distinguish between different types of transport models. Observation of a steepening of the radio spectrum at a point in a lobe relative to that in the hot spot can be used to infer a time, T, since the electrons were accelerated. If this point in the lobe is a distance L from the hot spot, we may calculate a characteristic speed $V = L/T$. If the resultant speeds are in the range (5–60) $\times$ 10^3 km s^{-1}, we may conclude that the observations are consistent with the simple version of the beam model. If speeds substantially higher than 60 $\times$ 10^3 km s^{-1} are obtained, we may conclude that the energetic electrons stream rapidly out of the hot spot.

An obvious alternative interpretation for high separation speeds would be the occurrence of *in situ* acceleration processes (e.g., Eilek and Henrikson 1984). Observationally, we are unable to distinguish between high-streaming speeds and low-streaming speeds with reacceleration, since in both cases the net result is reduced synchrotron radiation losses. On the other hand, if the observations indicate low-streaming speeds, we may contend that *neither* fast streaming nor reacceleration is important.

In this paper we undertake an analysis of the sort outlined above. In § II we describe the calculations of spectral steepening, present graphs which are used in the analysis of spectral index data, and define parameters which determine the spectral behavior. In § III we discuss the choice of observational material and the method of data analysis. A detailed discussion of the results for five luminous radio galaxies is presented in § IV. A discussion of the results as a whole and potential corrections to our speed estimates are given in § V. A limited, but detailed, comparison with the numerical beam models is given in § VI. Finally, in § VII our conclusions are presented.

II. SPECTRAL STEEPENING DUE TO SYNCHROTRON RADIATION LOSSES

The radio spectrum resulting from an ensemble of electrons which is evolving due to synchrotron radiation losses has been discussed in numerous reference works (e.g., Kardashev 1962; Pacholczyk 1970). In this section we present the results in a form convenient for application to Very Large Array (VLA) observations. Scaled-array VLA observations can produce credible, high-resolution spectral index maps of radio sources. We therefore hope that the results presented in this paper will be of use to many VLA observers.

An electron spectrum subject to synchrotron radiation losses is given by (Pacholczyk 1970, chap. 6)

$$N(E, \theta, t) = N_0 E^{-\gamma}[1 - C_2 B^2(\sin^2 \theta)Et]^{\gamma - 2} . \quad (1)$$

Here $N(E, \theta, t)$ is the differential electron spectrum which is a function of energy (E), pitch angle, (θ), and time (t) since losses commenced, which we identify with the time since acceleration. The initial energy spectrum is assumed to be a power law.

The electron spectrum normalization factor is N_0, and the initial electron spectrum spectral index is γ.

The quantity C_2 is a constant defined by Pacholczyk (1970), and B is the magnetic field strength. The intensity of synchrotron radiation resulting from a source possessing an electron spectrum of the form in equation (1) is given by (Pacholczyk 1970)

$$I_\nu(t) = 4\pi C_3 N_0 sB \int_0^{\pi/2} d\theta \sin^2 \theta \int_0^{E_T} dE\, F(x) E^{-\gamma} \times [1 - C_2 B^2(\sin^2 \theta)Et]^{\gamma - 2} ,$$

$$E_T \equiv [C_2 B^2(\sin^2 \theta)t]^{-1} . \quad (2)$$

In equation (2) we have assumed an isotropic pitch-angle distribution. The thickness of the source is given by s. The parameter C_3 is another constant defined by Pacholczyk (1970), as are the function $F(x)$ and the characteristic frequency ν_c, where $x \equiv \nu/\nu_c$.

The derivation of equation (2) assumes that electrons maintain the same pitch angle throughout their radiative lifetime. We shall hereafter refer to equation (2) as the Kardashev-Pacholczyk (KP) model. Jaffe and Perola (1974) assumed that electrons are isotropized on time scales short compared with their radiative lifetimes. In this case, the term $C_2 B^2(\sin^2 \theta)Et$ in equation (2) should be replaced by $C_2 B^2\langle \sin^2 \theta \rangle Et$, where $\langle \sin^2 \theta \rangle$ represents the time-averaged pitch angle. Equation (2) so modified will be referred to as the Jaffe-Perola (JP) model.

Inasmuch as we are nearly totally ignorant of the microphysics of extragalactic radio sources, we shall not argue in favor of the KP or JP model but instead shall consider them as limiting cases of these microscopic processes. For convenience we will generally cite results from the KP model, but will comment on the corresponding JP values as well. As will be seen below, the resultant separation speeds are remarkably insensitive to the microscopic model.

Equation (2) does not include the effect of expansion losses. We first note that inclusion of such effects is not straightforward in the case of a double radio source. Jaffe and Perola (1974) studied the case of an expanding plasma cloud, in which the adiabatic losses may be accommodated. For the lobe of a double radio source, electrons probably experience expansion losses upon egress from the compressed region associated with the hot spot. Calculation of these losses would be difficult and is at any rate beyond the scope of this paper.

By way of justification for this neglect, we make two apologies. First, expansion losses will produce observational effects which tend to exaggerate synchrotron losses. A discussion recognizing this fact will be presented in § V. Second, as will be discussed in § III, we have restricted our analysis to portions of radio lobes where expansion losses are arguably small.

For simplicity, we have assumed a constant magnetic field strength. The variation in the equipartition magnetic field strength throughout a lobe is quite small, except in regions where our neglect of adiabatic losses is obviously invalid, and our analysis inapplicable.

We have numerically solved equation (2) for both the KP and JP models. Since this is a straightforward and precedented enterprise, we forgo presentation of the numerical details and proceed to present our results.

The quantities observable on a radio map are the (normalized) radiation intensity at a given frequency, and the radio spectral index between two frequencies. These quantities are functions of two variables: γ, the spectral index of the energetic electron spectrum, and a parameter we define as X_0, which is a measure of the maturity of synchrotron radiation losses.

The definition of X_0 is

$$X_0 = \frac{C_2^2}{C_1} \nu B^3 t^2 , \tag{3}$$

where C_2 and C_1 are constants defined by Pacholczyk (1970), ν is the radio frequency, B is the magnetic field strength, and t is the time since radiation losses commenced. In more convenient units, equation (3) becomes

$$X_0 = 8.9 \times 10^{-4}(1 + z)\nu_{\rm GHz} B_{-5}^3 t_{\rm Myr}^2 . \tag{4}$$

In equation (4) z is the redshift of the source, $\nu_{\rm GHz}$ is the frequency of observation in GHz, B_{-5} is the magnetic field strength in units of 10^{-5} G, and $t_{\rm Myr}$ is the time in millions of years. For the JP model, the right-hand sides of equations (3) and (4) should be multiplied by $\langle \sin^2 \theta \rangle^2$.

In Figure 1 we display the normalized intensity of a homogeneous synchrotron source as a function of $X_0^{1/2}$ for the KP model. The use of $X_0^{1/2}$ rather than X_0 will be justified below. To choose an example to illustrate the use of this plot, we see that if the energetic electron spectrum is initially proportional to $E^{-5/2}$, the intensity will have fallen to half of its initial value when $X_0 = 0.42$.

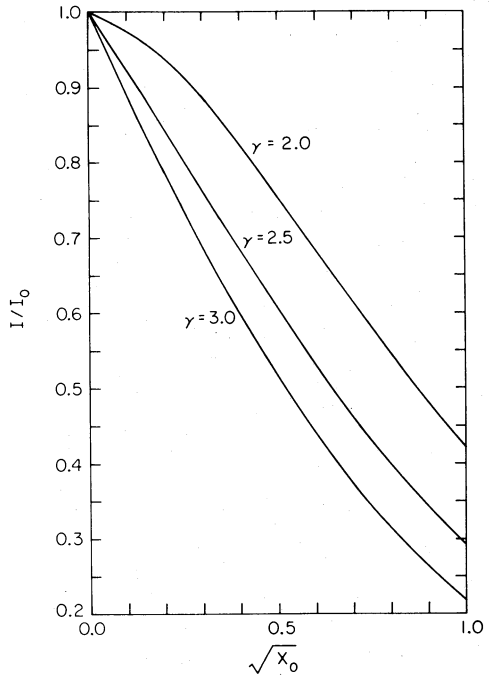

FIG. 1.—Normalized radio intensity as a function of the parameter X_0 (defined in eqs. [3] and [4] of the text). We assume a homogeneous source with an isotropic electron pitch-angle distribution.

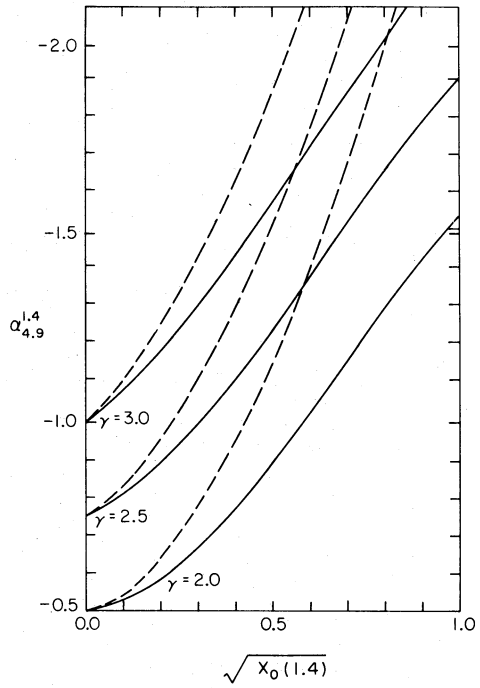

FIG. 2.—Spectral index between 1.446 and 4.885 GHz (standard VLA observing frequencies) as a function of X_0 at 1.446 GHz. The three curves correspond to electron spectral indices of 2.0, 2.5, and 3.0.

The two-point spectral index is a better indicator of synchrotron losses than the total intensity. The total intensity obviously changes as the thickness of the source changes. This is not true of the spectral index. Furthermore, the total intensity is more sensitive to expansion losses than the spectral index. For these reasons, the analysis in this paper concentrates on the two-point spectral index as an observable.

We anticipate that most future studies of spectral steepening in extragalactic radio sources will utilize observations made with the VLA radio telescope. We therefore present our results in terms of spectral indices between the standard VLA observing frequencies of 1.446, 4.885, and 15.0 GHz, frequencies for which the scaled-array mode of operation can be used.

The first such plot is shown in Figure 2. The ordinate is the value of $X_0^{1/2}$ at 1.446 GHz. The abscissa is the spectral index between 1.446 and 4.885 GHz. Different curves represent cases with $\gamma = 2$, 2.5, and 3.0; solid and dashed curves represent the KP and JP models, respectively. Given a measurement of the 1.446–4.885 GHz spectral index, and a knowledge of the initial spectral index, Figure 2 can be used to determined X_0, and thus, by equation (4), the product $B_{-5}^3 t_{\rm Myr}^2$, for either the KP or the JP model.

Figure 3 is identical with Figure 2, except that the spectral index is now that between 4.885 and 15.0 GHz, and X_0 is defined at 4.9 GHz.

Figures 2 and 3, together with equation (4), may be used to estimate the time since acceleration of the electrons. In keeping with the goals of this paper, we would like to relate observable parameters to the relative speed between the hot spot and lobe material. From equation (4), we see that a change in $X_0^{1/2}$ can be related to a change in the age of the electrons:

$$d(X_0^{1/2}) = 0.03[(1 + z)\nu_{\rm GHz}]^{1/2} B_{-5}^{3/2} dt_{\rm Myr} . \tag{5}$$

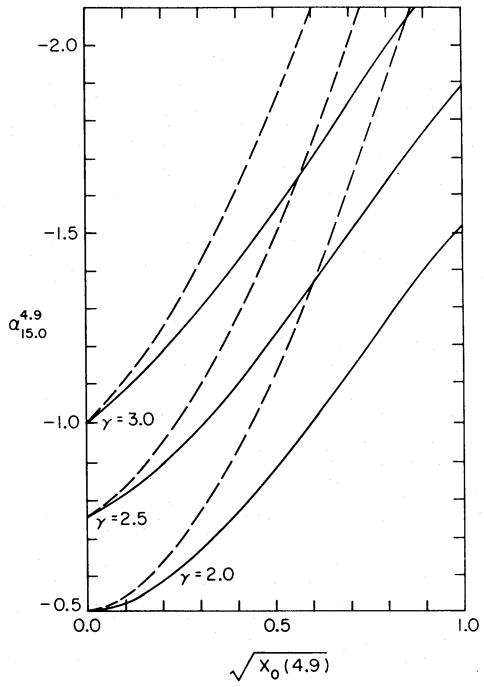

FIG. 3.—Same as Fig. 2, except the ordinate is the spectral index between the standard VLA observing frequencies of 4.885 and 15.0 GHz.

Equation (5) has motivated the use of $X_0^{1/2}$, rather than X_0, as a convenient parameter for analysis.

We may define an instantaneous separation speed, $V_s(\tau)$, as

$$V_s(\tau) = \left.\frac{dL}{dt}\right|_{t=\tau} = 10^3 \left.\frac{dL_{\rm kpc}}{dt_{\rm Myr}}\right|_{t=\tau} \text{ km s}^{-1}, \quad (6)$$

where dL is the change in separation of the hot spot and lobe material. Combination of equations (5) and (6) provides us with the following formulae:

$$\frac{d(X_0^{1/2})}{dL_{\rm kpc}} = \frac{30[(1+z)\nu_{\rm GHz}]^{1/2}B_{-5}^{3/2}}{V_s}, \quad (7a)$$

or

$$V_s = 30[(1+z)\nu_{\rm GHz}]^{1/2}B_{-5}^{3/2}\left(\frac{d(X_0^{1/2})}{dL_{\rm kpc}}\right)^{-1} \text{ km s}^{-1}, \quad (7b)$$

where, in general, V_s and $d(X_0^{1/2})/dL_{\rm kpc}$ may be evaluated on a point-by-point basis.

Equations (7) provide the crux of our analysis. Our modus operandi is as follows. From dual-frequency VLA maps we measure the spectral index as a function of position from the hot spots. Using Figures 2 and 3, we may infer a value for X_0 at each point in the lobe. Such data may be used to obtain a best value and plausible range for the slope $d(X_0^{1/2})/dL_{\rm kpc}$.) These measurements yield, via equation (7b), estimates for the separation speed. Our practice has been to use these speed estimates to calculate expected spectral indices which can be compared with the data. This permits one to ascertain a value for the speed of separation and also to appreciate how well the data conform to a constant speed of separation.

From equation (7b) we see that the separation speed is determined entirely by observable properties, with the exception of the magnetic field strength. For this quantity we naturally use the equipartition magnetic field strength, there being no alternative.

At this point it is worthwhile to compare the separation speeds obtained by the KP and JP models. We will indicate the differences by an example. Let us assume that the spectral index of a source is observed to steepen from -0.75 to -1.20 over some distance. From Figure 2 we see that, according to the KP model, $d(X_0^{1/2}) = 0.48$, whereas for the JP model $d(X_0^{1/2}) = 0.35$. This would seem to indicate that the JP streaming speed is about 40% higher than the KP value, but it must be recalled that the JP expression for $X_0^{1/2}$ differs from the KP value by a factor of $\langle \sin^2\theta \rangle$. For an isotropic pitch-angle distribution, $\langle \sin^2\theta \rangle = \frac{1}{2}$, so we conclude that the JP separation speed is 30% lower than the KP value. This model-dependent uncertainty is less than that introduced by a host of other effects listed in § V, so the choice of a pitch-angle distribution model does not affect our conclusions.

In an ambitious undertaking, one might hope to use Figures 2 and 3 to distinguish between the KP and JP models, and thus obtain information on the electron pitch-angle distribution. Measurements in regions of large spectral index would be required.

We close this section by relating the aforementioned analysis to our goal, which is elucidation of electron transport processes in double radio sources. From observational data and the assumed validity of the equipartition magnetic field, we can estimate separation speeds by using equation (7b). If these speeds are in the range (5–60 $\times$ 10^3 km s^{-1}, we would conclude that the simplest form of the beam model, discussed in § I, accounts adequately for the observations. If the inferred speeds greatly exceed the 60 $\times$ 10^3 km s^{-1} limit of Longair and Riley (1979), models of electron transport including free streaming would be favored.

III. CHOICE OF OBSERVATIONAL MATERIAL AND METHODS OF DATA ANALYSIS

The data used in our investigation consist of 1.446 and 4.885 GHz, scaled-array VLA observations of five 3C radio galaxies. The sources are 3C 79 (Spangler, Myers, and Pogge 1984), 3C 166 (Spangler and Bridle 1982), 3C 379.1 (in preparation), 3C 411 (Spangler and Pogge 1984), and 3C 430 (Spangler, Myers, and Pogge 1984). These sources were chosen for observation on the basis of possessing extended lobe or radio bridge emission. The existence of emission at substantial distances from the hot spots renders these sources particularly well suited for study relevant to this paper. Descriptions of the observations and methods of data analysis can be found in the cited papers.

Table 1 lists the sources for which analysis was undertaken. Our data sample consists of seven lobes in five sources. We have attempted to furnish enough information for interested

TABLE 1

RADIO LOBES FOR SYNCHROTRON-AGING ANALYSIS

Source	z	$\theta_{\rm FWHM}$ (arcsec)	Scale (kpc arcsec^{-1})	Lobe	$B_{\rm eq}$ ($\times 10^{-5}$ G)
3C 79	0.256	1.5	2.5	Sf	2.2
3C 166	0.246	1.6	2.5	S	2.0
3C 379.1	0.256	4.0	2.5	Np	1.2
3C 379.1	...	...	...	Sf	1.2
3C 411	0.469	1.5	3.5	Sf	5.0
3C 430	0.055	1.8	0.67	Sp	2.1
3C 430	...	...	...	Nf	2.2

readers to reanalyze our data, given information contained in this paper.

The first column of Table 1 gives the source name, and the second column the redshift, as tabulated by Burbidge and Crowne (1979). The third column lists the angular diameter (FWHM) of the restoring beam used in the data reduction. The image scale used in our analysis is given in column (4), and assumes an Einstein–de Sitter universe with $H_0 = 100$ km s^{-1} Mpc^{-1}. Column (5) gives the lobe designation; for 3C 379.1 and 3C 430 both lobes were analyzed.

Column (6) gives our estimate of the equipartition magnetic field strength in the lobe of each source, which we will assume equals the true magnetic field strength. From equation (7b) we see that the inferred separation speeds are proportional to the 3/2 power of the magnetic field strength, so additional comment on this parameter is in order.

For each source, this quantity was calculated in the lobe or radio bridge, the portion of the source that is of interest to our study. The equipartition magnetic field is determined by the radiation intensity and the physical depth of the source. We model the lobes and radio bridges as homogeneous cylinders viewed perpendicular to the cylinder axis. Measurements of the radio intensity were made along a slice perpendicular to the source axis, and fit in a least squares sense to the radiation from a homogeneous cylinder. The quantities resulting from the fit were the central intensity and diameter of the cylinder, which we used for the thickness of the source.

Calculations of equipartition magnetic field also require an assumption concerning the low-energy cutoff of the electron spectrum. It is conventional in the literature to equate this cutoff with electrons which radiate at 10 MHz, the lowest frequency at which extensive flux density measurements have been made. While such a convention is justifiable for those who desire a "minimum energy" magnetic field, it is clearly arbitrary and unrealistic, and leads to an underestimate of the true magnetic field strength if equipartition is in effect. We have therefore assumed that the energetic electron spectrum extends to a minimum energy of 10 MeV. While arbitrary, it is hoped that this convention leads to a more realistic estimate of the magnetic field strength. It should be noted, however, that our estimates are only slightly (a factor of 2 or less) higher than those calculated with the more conventional recipe.

Further conventions developed for the analysis of map data may be discussed in reference to Figure 4, which displays a 1.446 GHz map of 3C 379.1, of higher resolution than that used in our analysis. The dark lines represent the "slices," or lines along which measurements of intensity and spectral index were made for analysis. For 3C 379.1 as well as the remainder of our sources, measurements were made along the axis of the lobe or radio bridge, a choice dictated by our model of a homogeneous cylinder.

For all of our sources, the total intensity displays similar behavior along the lobe axis. The total intensity is highest in the hot spot, and drops precipitously upon egress from the hot spot. With increasing distance from the hot spot, the intensity shows a very gradual decrease. This behavior may be clearly seen in the slices displayed in § IV below.

We propose the following interpretation for this apparently general characteristic. Electrons are accelerated in the high-density region associated with the hot spot. The beam model associates the hot spots with the shocks produced by beam impact with the intergalactic medium, so higher densities are expected. As the electrons flow out of the hot spot, they should expand, resulting in adiabatic losses. In the far-downstream region which we associate with the lobe, expansion losses cease or are greatly diminished; the lobe regions typically can be thermally confined by intergalactic medium gas. Synchrotron radiation losses are then important in the lobes. In support of these notions, we point out that in 3C 79, 3C 166, and 3C 430 the spectral index does not change as one leaves the hot spot, even though the intensity drops substantially. Such behavior is inconsistent with synchrotron losses and suggests expansion losses. Another possibility is strong inhomogeneity in the source, i.e., a substantial drop in the magnetic field strength.

Neither of these mechanisms (expansion losses and source inhomogeneities) is accounted for in the model discussed in § II, and indeed both would be difficult to describe realistically. We have therefore restricted our attention to the remote lobe region, where we can at least hope that the assumptions of our analysis (homogeneity of the source region, dominance of synchrotron losses) are approximately obeyed.

One disadvantage of this approach is that substantial subjectivity is introduced in the choice of the region where analysis is to be undertaken.

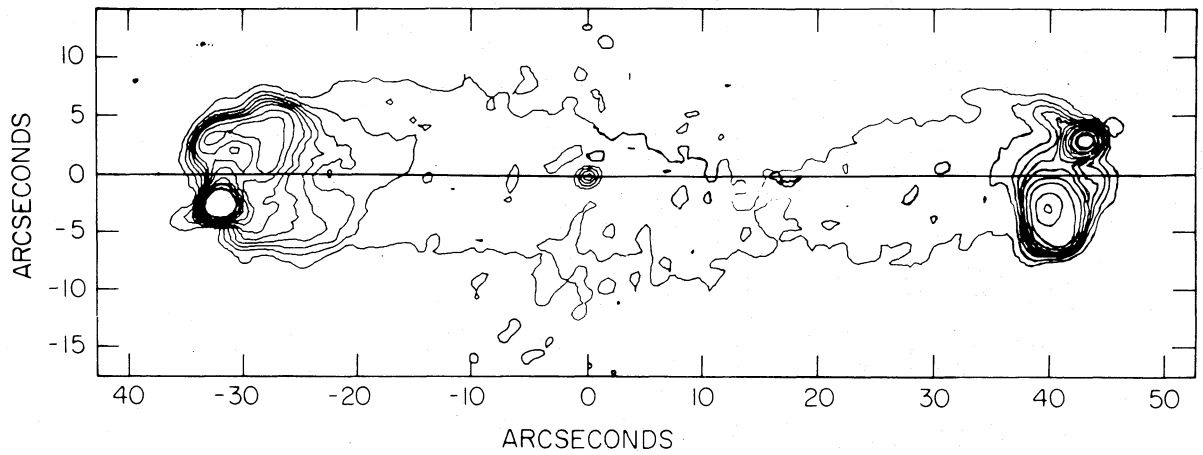

FIG. 4.—A 1.446 GHz map of the source 3C 379.1. The resolution is 2″0 (FWHM). Contours are plotted at −0.25% (*dashed contour*), 0.25%, 0.75%, 1.25%, 1.75%, 2.25%, 2.75%, 3.75%, 5.0%, 7.5%, 10.0%, 12.5%, 18.75%, and 22.5% of the peak intensity, which is 0.24 Jy beam^{-1}. The lines represent slices along the lobe axes on which spectral index and total intensity measurements were made.

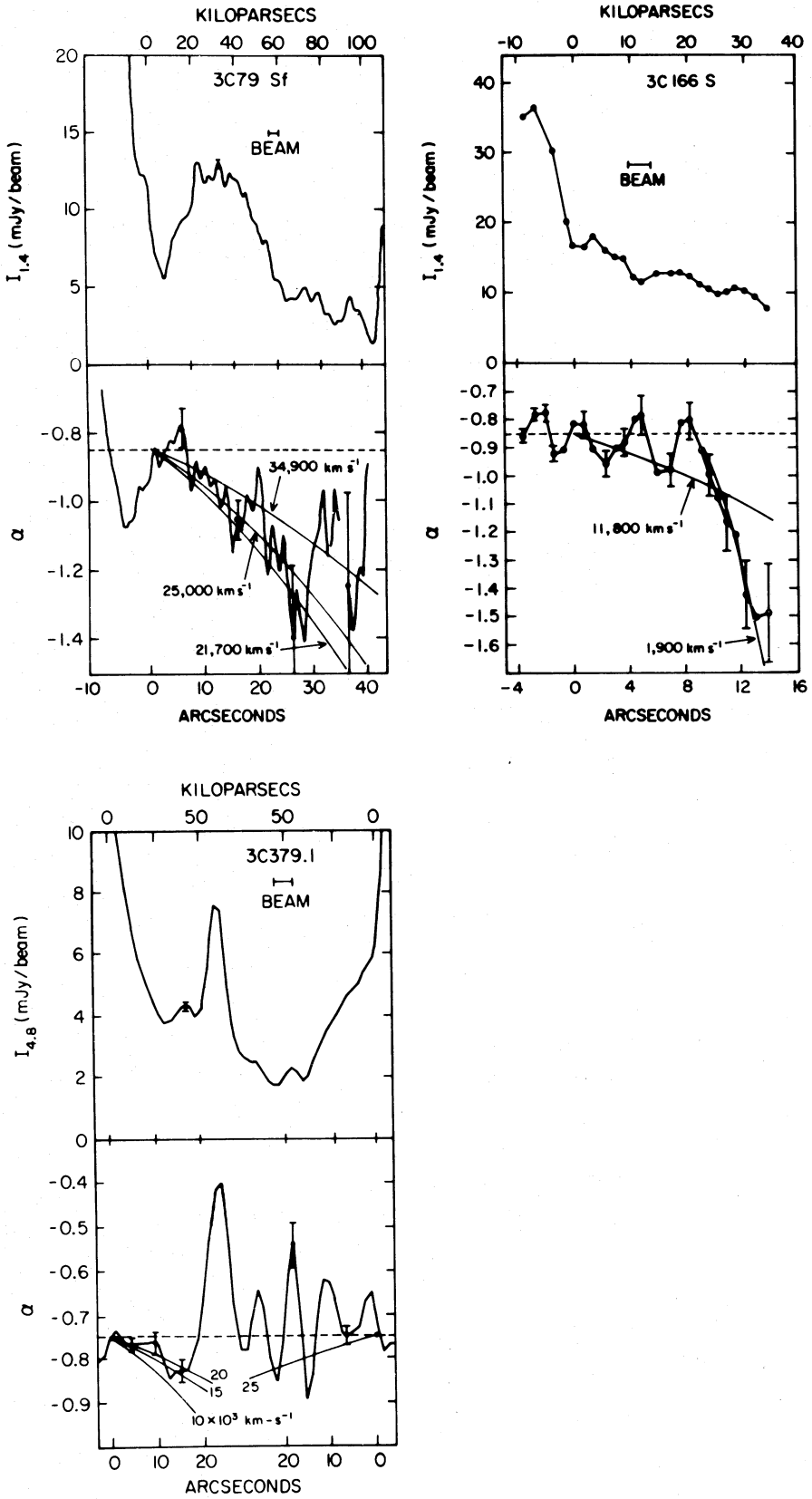

FIG. 5.—Total intensity and spectral index measurements along the axes of 3C 79, 3C 166, and 3C 379.1 (both lobes). Solid curves begin at the point where we conjecture that synchrotron radiation losses become dominant. The solid curves represent the spectral indices expected for constant separation speeds.

IV. RESULTS OF THE ANALYSIS

In this section, we discuss the measurements of each of the seven lobes listed in Table 1 and consider the evidence for hot spot motion or particle streaming.

a) 3C 79

Our results for the south-following (Sf) lobe of 3C 79 are presented in the upper left-hand set of panels of Figure 5. The same format will be used for all subsequent sources. The top panel presents the 1.446 GHz intensity along the axis of the Sf lobe. The slice displays the very high intensity associated with the hot spot, followed by a region characterized by more gradual changes in intensity. Inspection of the map of 3C 79 (Spangler, Myers, and Pogge 1984) suggests that at least part of the enhancement near the center of the slice may be due to a widening of the source at this point. This spoils the intensity data for quantitative uses, but should not affect the utility of the spectral index data.

Measurements of spectral index along the same slice are shown in the lower panel.

The solid curves begin at a point at which we think synchrotron losses are dominant, and represent the expected spectral indices for various separation speeds. We see that a speed of 25×10^3 km s^{-1} provides a good fit to the data, with a permissible range of (22–35) $\times 10^3$ km s^{-1}.

b) 3C 166

The data for the south lobe of 3C 166 are shown in the upper right hand set of panels in Figure 5. Solid curves again represent the expected spectral indices for different speeds of separation.

A constant speed of separation between hot spot and lobe material cannot account for our observations of 3C 166. The pronounced spectral steepening in the back of the lobe suggests separation speeds of order 1900 km s^{-1}. Further up, in the first 6″ of the slice, separation speeds of about 12×10^3 km s^{-1}, or greater, are indicated. The data shown in Figure 5 could be accounted for if the hot spot speed of advance is now higher than it was in the past.

c) 3C 379.1, Np Lobe

The low intensity of the lobe radiation in this source required the use of a lower resolution map, so both lobes are shown in Figure 5, the north-preceding (Np) lobe being to the right and the Sf lobe to the left. The total intensity measurements are at a frequency of 4.8 GHz.

The spectral index data shown in Figure 5 provide no convincing evidence of a spectral index gradient; the plotted curve represents an upper limit to the plausible spectral index gradient. A lower limit to the streaming speed of about 25×10^3 km s^{-1} is indicated.

d) 3C 379.1, Sf Lobe

A small but detectable spectral index gradient is seen, corresponding to a separation speed of about 17×10^3 km s^{-1}, with a permissible range of (15–20) $\times 10^3$ km s^{-1}.

e) 3C 411, Sf Lobe

The observations of 3C 411, shown in Figure 6, show a change in spectral index upon egress from the hot spot, with relatively minor subsequent variations. In this case, relatively high separation speeds seem indicated. These high speeds, however, may be an artifact of the high adopted value for the magnetic field.

Further VLA observations, at a frequency of 15 GHz, have been made of 3C 411 and are presently under study. Preliminary results indicate a gradient in the 4.9–15 GHz spectral index which is indicative of a separation speed comparable to the low end of the range presented here.

f) 3C 430, Sp Lobe

The spectral index data show reasonable conformity with a constant speed of separation of about 15×10^3 km s^{-1}. The permissible range is (8–20) $\times 10^3$ km sec.

g) 3C 430, Nf Lobe

The spectral index measurements are in reasonable agreement with a constant separation speed in the range (8–20) $\times 10^3$ km s^{-1}, and a best value of about 11×10^3 km s^{-1}. Within the considerable uncertainty, the hot spot speeds of advance are the same in the two lobes. The curves plotted with the total intensity data result from an attempt to use the total intensity data to determine X_0, i.e., use of Figure 1. The inferred speeds are seen to be considerably less than those deduced from the spectral index data. This indicates that processes other than synchrotron losses are responsible for at least part of the decline in total intensity.

V. DISCUSSION

The results of § IV are summarized in Table 2. Columns (1) and (2) indicate the source and lobe. Column (3) lists our estimate of a separation speed which is generally consistent with the spectral index data. Column (4) lists the range of plausible separation speeds. Once again, we note that the JP speeds would be about 70% of those listed in Table 2.

The results in Table 1 are in satisfactory agreement with the simplified version of the model discussed in § I. For the most part, the speed estimates fall in the (5–60) $\times 10^3$ km s^{-1} range described in § I. Our separation speeds are comparable to those obtained for similar sources, in independent analyses by Burch (1977, 1979) and Winter *et al.* (1980). There are no compelling instances of separation speeds in excess of the 60×10^3 km s^{-1} limit, which should be considered the firmer limit. The only potential embarrassment to the beam model arises from 3C 166. The speed of $\sim 2 \times 10^3$ km s^{-1} which characterizes the lobe periphery is below that which would be expected if the hot spots are ram-pressure–confined.

Even 3C 166 may not present a major problem, however. The portion of the lobe characterized by this low separation speed is relatively close to the nucleus. Such a region may contain gas densities greater than those in the intergalactic medium, so it is quite plausible that the hot spot speed of advance was indeed considerably less in the past.

TABLE 2

SUMMARY OF SEPARATION SPEEDS

Source	Lobe	V_s (km s^{-1})	V_s Range (km s^{-1})
3C 79	Sf	25,000	20,000– 35,000
3C 166	S	12,000	2,000– 15,000
3C 379.1	Np	>25,000	>25,000
3C 379.1	Sf	17,000	15,000– 20,000
3C 411	Sf	60,000	40,000–100,000
3C 430	Sp	15,000	8,000– 20,000
3C 430	Nf	11,000	8,000– 20,000

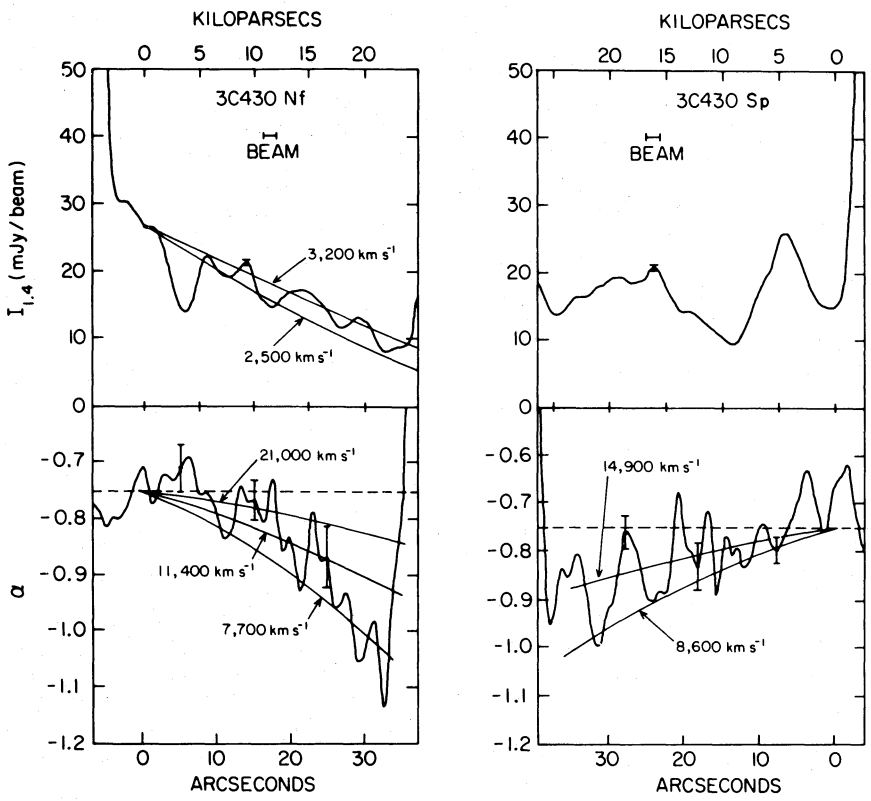

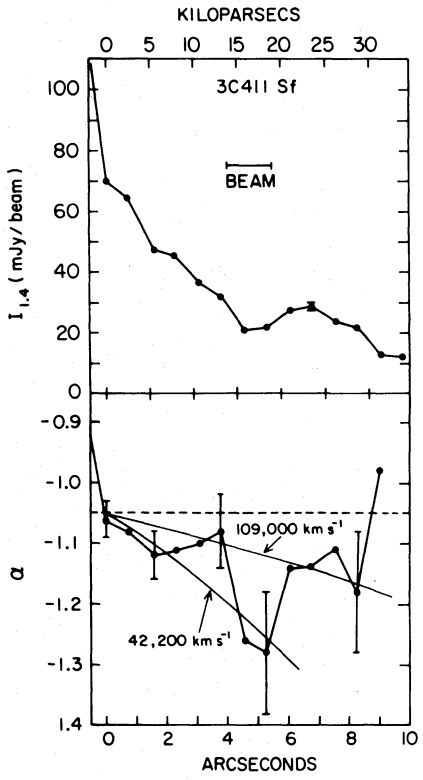

FIG. 6.—Same as Fig. 5, except for 3C 411 and 3C 430 (both lobes)

We now wish to consider a number of corrections to the above separation speeds which have not been included in our analysis. A major motivation is as follows. The separation speeds in Table 2 are sufficiently low that, taken by themselves, they serve to practically exclude models of electron transport based on free particle streaming. Stated differently, the speeds of separation are so much smaller than the kinetic speed of the electrons that the electrons must be confined and not capable of free motion. If three-streaming models are to be viable, substantial corrections must be made to the speeds listed in Table 2. We now attempt an assessment of various modifications to our speeds.

a) Projection Effects

Projection effects unquestionably result in our underestimating the speed of separation. What we measure is the projection on the plane of the sky of the distance between the hot spot and a point in the lobe; our analysis assumes the source to be in the plane of the sky. For a random sample of sources with a uniform distribution of angles between the source axis and the plane of the sky, we would expect a correction to the distance of 1.27, and a similar correction to the deduced speeds of separation. This correction should be applied to the mean speed of the sample.

b) Adiabatic Losses

As discussed in §§ II and III, we attempted to choose for analysis portions of the lobes where we suspected minor adiabatic losses. It is important to assess the effect of the remaining adiabatic losses. If a spectral index gradient due to synchrotron losses has occurred, adiabatic losses will move the "synchrotron break" to lower frequencies, thus mimicking continued synchrotron losses. The net effect is that one overestimates X_0, and thus underestimates the speed of separation.

One can assess the possible role of adiabatic losses with the data shown in Figures 5 and 6. From these figures we see spectral index changes, $\Delta\alpha$, which are typically in the range 0.3–0.4. Referring to Figure 2, we see that this suggests changes in $(X_0^{1/2})$ of order 0.3–0.4. Figure 1 then indicates that we should expect the 1.446 GHz intensity to decline by about 25%–30% (for $\gamma = 5/2$) if synchrotron radiation losses alone were operative. The actual intensity declines are slightly larger than this, being 40%–50% in the cases of 3C 166 and 3C 430. We take this as evidence that our approximation of dominant synchrotron radiation losses is reasonably good, but that a small correction to X_0 is needed to account for the residual expansion losses. A simple analysis, based on the theory of Pacholczyk and Scott (1976), indicates that if a factor of 2 drop in total intensity is caused by expansion losses, we would overestimate the time since acceleration by 30%. Such errors are negligible compared with other uncertainties.

c) Image Scale

In our analysis we have assumed a Hubble constant of 100 km s^{-1} Mpc^{-1}. If a value of 50 km s^{-1} Mpc^{-1} is correct, then the length scales and separation speeds should be raised by a factor of 2. Aside from recognition of this fact, discussion is obviously beyond the scope of this paper.

d) Magnetic Field Strength

The true strengths of the lobe magnetic fields remain one of the greatest uncertainties in our analysis. As may be seen from equation (7), our separation speed estimates are proportional to the 3/2 power of the field strength. If our field estimates are too high, the inferred streaming speeds might be sufficiently low to cause problems for the beam model. On the other hand, it is worth pointing out that at least one of the "free-streaming" models, that of Spangler (1979) and Spangler and Basart (1981) requires magnetic field strengths in excess of the equipartition value. Specifically, the model requires field strengths of order 10^{-4} G (Spangler 1979). It is obvious that if the field is indeed this strong, then the requisite high streaming speeds are also obtained.

e) Source Filling Factor

Recent high-resolution, high dynamic range maps of Cygnus A (Perley, Dreher, and Cowan 1984) show a highly filamentary structure. The volume-filling factor is estimated to be in the range 0.03–0.3. Low filling factors raise estimates of the equipartition magnetic field. If filling factors in the sources considered in our analysis are similar to those in Cygnus A, then the magnetic fields are higher by a factor of 1.4–2.7, and the separation speed is raised by a factor of 1.6–4.4.

f) Magnetic Field Topology

The detailed structure of the magnetic field is of importance only to models which invoke particle motion along a large-scale magnetic field. The speed of separation, which is equivalent to the electron-streaming speed in the streaming models, has been calculated by dividing the distance to the hot spot by the synchrotron age of the electrons. This convention *assumes* straight-line propagation from the hot spot to the lobe region, which would occur if the lobe is permeated by a straight, static magnetic field which is parallel to the source axis.

Interferometric polarization observations of the lobes of doubles, including those discussed in this paper, reveal substantial departures of the fractional linear polarization from the value expected for radiation in a uniform magnetic field. These observations are plausibly interpreted by positing a large-amplitude, random magnetic field component which is superposed on the uniform component. Observations indicate that the amplitude of this random component must be comparable to or larger than the uniform component.

The implication of this observation is that a charged particle moving along the magnetic field will not travel in a straight line but will follow the meandering magnetic field line. The resultant increase in the path length depends on the statistics of the magnetic fluctuations. An expression has been derived for the path-length enhancement, using the approach developed by Hollweg and Jokipii (1972) in a quite different application. For Gaussian-distributed fluctuations with characteristics dictated by observations, the path-length (and thus separation-speed) enhancement is a factor of 1.5–2. However, for other fluctuation probability distributions, an arbitrary enhancement may occur.

It should be noted that for this mechanism to redeem the streaming models, it would be necessary for the fluctuations to be large scale. If significant power exists on scales comparable to the electron gyroradii, pitch-angle isotropization would occur, and streaming would be limited to the (rather low) Alfvén speed.

We feel that, depending on the magnitude of the aforementioned corrections, either the simplified beam model or the electron-streaming models are compatible with the observations. In favor of the beam model we note that our initial estimates of separation speed, given in Table 2, are close to those predicted. If the true magnetic field strength is close to

our equipartition field estimates, then the agreement of prediction and observation will be maintained. Adiabatic losses should have a small effect on our analysis. The viability of the simplified beam model would be reduced if any of the aforementioned six modifications are significant, or if a number of them act in concert. Reference to Table 2 indicates that the net effect of all modifications must be less than 5–6 for the simplified beam model to remain viable.

Free-streaming models begin with the disadvantage that the initial estimates for the streaming speed given in Table 2 are considerably below the model's requirements. One is therefore required to invoke substantial correction factors to the inferred streaming speeds. One such effect is the magnetic field strength. Models which posit electron streaming along a magnetic field require the field to exceed the equipartition field, so substantial corrections to the electron-streaming speed would be expected. An increase in path length due to a spatially fluctuating magnetic field would also lead us to underestimate the true streaming speed. These two effects could easily result in a correction factor of 10 or greater, in which case the observations are entirely compatible with the theory.

The desire for simplicity naturally leads one to favor the simplified beam model. We conclude this section by pointing out an interesting feature of 3C 430 which would be profitably sought in other sources. The hot spots in this source are about equidistant from the central component, the ratio of distances being about 1.09 with the Nf hot spot being more distant. A ratio closer to unity is obtained if one measures the distance from the central component to the extreme edge of each lobe. This indicates that the hot spot speed of advance is very similar in the two lobes.

Our measured separation speeds are a combination of the hot spot speed of advance and the speed at which electrons stream out of the hot spot. Our observations indicate that the separation speeds are very similar in the two lobes. We conclude that either (*a*) the streaming speed is small compared with the hot spot speed of advance or (*b*) the streaming speeds are very similar in the two lobes.

Polarization observations of this source (Spangler, Myers, and Pogge 1984) argue against the second possibility. The Nf lobe is characterized by low fractional linear polarization at 4.885 GHz and depolarization between 1.4 and 5 GHz. The Sp lobe has higher fractional polarization at 5 GHz and little or no depolarization. One would therefore expect the electron transport processes to be quite different in the two lobes. Our observed result that the separation speeds are quite similar in the two lobes therefore indicates that electron streaming or diffusion does not play an important role, and that the measured separation speed is equal to the hot spot speed of advance.

To qualify this result, we point out that 3C 430 is at a low galactic latitude, and displays Faraday rotation fluctuations which may be of galactic origin (Spangler, Myers, and Pogge 1984). It is therefore possible that our observations are affected by depolarization in a foreground screen. Similar analyses on other sources would therefore be desirable.

VI. COMPARISON WITH NUMERICAL STUDIES OF THE BEAM MODEL

In the simplified beam model presented above, energetic electrons are left behind a moving hot spot, so the measured separation speed equals the hot spot speed of advance through the intergalactic medium. This is obviously an oversimplified description of matters, and it would be worthwhile to make a comparison with more refined models. The recent numerical experiments of Norman *et al.* (1982), and of Norman, Winkler, and Smarr (1983) provide such models.

A common feature of the sources analyzed in §§ III and IV is the existence of a radio bridge or extended lobe. According to the beam model, these bridges correspond to "cocoons" formed by material which has flowed through the strong shock associated with the hot spot and is now experiencing backflow.

Norman *et al.* (1982) and Norman, Winkler, and Smarr (1983) demonstrate that extensive cocoons form only for beams which are less dense than the ambient medium and have high Mach numbers. For such beams, the speed of hot spot advance is roughly 3–10 times the sound speed in the background medium (Norman, Winkler, and Smarr 1983, Table 1). Such models are also characterized by strong backflow.

We consider as an example the calculation presented in Figure 5 of Norman *et al.* (1982), which consists of a Mach 6 jet possessing a density 10% of that of the background medium. The speed at which the hot spot moves into the intergalactic medium (IGM) is 4.2 times the sound speed in the IGM, or 3800 km s^{-1} if one assumes a "typical" IGM temperature of 10^8 K. A cocoon of roughly constant diameter is formed by a backflow of 7.2 times the sound speed, or 6500 km s^{-1}, measured in the rest frame of the IGM. The net separation speed of the hot spot and cocoon material, the quantity obtained from our spectral index measurements, is therefore 10,300 km s^{-1}.

The prediction of the model is therefore in quite favorable agreement with at least the lower range of experimentally determined separation speeds listed in Table 2. Furthermore, the results and scaling arguments presented in Norman *et al.* (1982) and Norman, Winkler, and Smarr (1983) indicate that higher separation speeds would result from higher Mach number jets. Further work, both observational and computational, is needed to more firmly establish this finding. However, it appears that the high Mach number, low-density jets can account for both the qualitative (existence of prominent, constant-diameter lobes) and quantitative (magnitude of spectral index gradient) properties of these radio galaxies.

VII. CONCLUSIONS

Measurements of 1.4–5 GHz spectral indices along the axes of several radio lobes in five radio galaxies have been used to determine the speeds of separation (or limits thereto) of hot spots and lobe material. For a simplified version of the beam model, described in § I, this separation speed is equal to the hot spot speed of advance through the intergalactic medium. For models in which electrons stream out of the hot spot along the source magnetic field, the separation speed is related to the electron-streaming speed. Our investigation has led to the following conclusions.

1. Inferred separation speeds are typically in the range (10–30) $\times$ 10^3 km s^{-1}. Such values are in good agreement with the simplified beam model.
2. The separation speeds are in good agreement with numerical simulations of beam models, provided that the beams are of lower density than the intergalactic medium, and are of high ($\gtrsim 5$) Mach number.
3. The separation speeds are lower than would be expected from electron-streaming models. For these models to be viable, one must contend that magnetic fields exceed the equipartition value and/or that the electrons follow wandering field lines.

This research was supported by grant AST82-17714 from the National Science Foundation.

REFERENCES

Blandford, R. D., and Rees, M. J. 1974, *M.N.R.A.S.*, **169**, 395.
Burbidge, G. R., and Crowne, A. H. 1979, *Ap. J. Suppl.*, **40**, 583.
Burch, S. F. 1977, *M.N.R.A.S.*, **180**, 623.
———. 1979, *M.N.R.A.S.*, **186**, 519.
Eilek, J. A., and Henrikson, R. N. 1984, *Ap. J.*, **277**, 820.
Hollweg, J. V., and Jokippi, J. R. 1972, *J. Geophys. Res.*, **77**, 3311.
Hughes, P. A. 1979, *M.N.R.A.S.*, **186**, 853.
Jaffe, W. J., and Perola, G. C. 1974, *Astr. Ap.*, **26**, 423.
Kardashev, N. S. 1962, *Soviet Astr.—AJ*, **6**, 317.
Longair, M. S., and Riley, J. M. 1979, *M.N.R.A.S.*, **188**, 625.
Lonsdale, C. J., and Morison, I. 1983, *M.N.R.A.S.*, **203**, 833.
Norman, M. L., Smarr, L., Winkler, H. A., and Smith, M. D. 1982, *Astr. Ap.*, **113**, 285.
Norman, M. L., Winkler, H. A., and Smarr, L. 1983, in *Astrophysical Jets*, ed. A. Ferrari and A. G. Pacholczyk (Dordrecht: Reidel), p. 227.
Pacholczyk, A. G. 1970, *Radio Astrophysics* (San Francisco: Freeman).
Pacholczyk, A. G., and Scott, J. S. 1976, *Ap. J.*, **210**, 311.
Perley, R. A., Dreher, J. W., and Cowan, J. J. 1984, *Ap. J. (Letters)*, **285**, L35.
Spangler, S. R. 1979, *Ap. J. (Letters)*, **232**, L7.
Spangler, S. R., and Basart, J. P. 1981, *Ap. J.*, **243**, 1103.
Spangler, S. R., and Bridle, A. H. 1982, *A.J.*, **87**, 1270.
Spangler, S. R., Myers, S. T., and Pogge, J. J. 1984, *A.J.*, **89**, 1478.
Spangler, S. R., and Pogge, J. J. 1984, *A.J.*, **89**, 342.
Wentzel, D. G. 1974, *Ann. Rev. Astr. Ap.*, **12**, 71.
Winter, A., *et al.* 1980, *M.N.R.A.S.*, **192**, 931.

STEVEN T. MYERS: Department of Astronomy, Code 105-24, California Institute of Technology, Pasadena, CA 91125

STEVEN R. SPANGLER: Department of Physics and Astronomy, University of Iowa, Iowa City, IA 52242